URANIUM AND THORIUM DECAY SERIES ISOTOPIC CONSTRAINTS ON THE SOURCE AND RESIDENCE TIME OF SOLUTES IN THE YELLOWSTONE HYDROTHERMAL SYSTEM

TIMOTHY P. MOLONEY ✦ KENNETH W. SIMS ✦ JOHN P. KASZUBA
UNIVERSITY OF WYOMING ✦ LARAMIE

✦ ABSTRACT

Hydrothermal fluids in Yellowstone National Park have widely varying chemical composition. Heat and volatile flux from the hydrothermal system can be estimated by monitoring the composition and volume of emitted hydrothermal fluid, but the source of solutes in hydrothermal fluid is often nebulous and the geochemical processes that affect the nuclides are poorly understood.

Measurements of ^{220}Rn and ^{222}Rn activity in hydrothermal fluids and of CO_2 flux from fumaroles and hot springs were carried out in Yellowstone National Park during the summer of 2010. We observed a weak relationship between (^{220}Rn/^{222}Rn) and CO_2 flux, which indicates that CO_2 acts as a carrier gas to bring radon to the surface, but the radon is sourced from aquifer rocks rather than magma. If radon reaching the surface were sourced from magma below Yellowstone, there would be a stronger correlation between (^{220}Rn/^{222}Rn) and CO_2 flux.

Measurements of ^{223}Ra, ^{224}Ra, ^{226}Ra, ^{228}Ra, and major solute chemistry in hot spring waters support the hypothesis that the time scale of solute transport from the deep hydrothermal reservoir is long compared to the half lives of ^{220}Rn and ^{222}Rn, which are useful for processes operating on the time scale of 5 minutes to 20 days. Radium isotope activities in hot springs indicate that the solute transport time varies significantly from region to region, indicating that circulation in some areas operates on the time scale of ^{224}Ra/^{223}Ra (20-55 days) and circulation in other areas operates on the time scale of ^{228}Ra/^{226}Ra (25-1600 years). The radium isotope composition of hot spring water is also influenced by differences in regional aquifer rocks and geochemical processes such as sorption and mineral precipitation. In summary, geochemical and hydrothermal processes in Yellowstone operate on many different time scales and in diverse geologic conditions, but radionuclide activities possess excellent potential to study these complex phenomena.

✦ INTRODUCTION

Geothermal monitoring in Yellowstone National Park (YNP) is important for volcanic hazard assessment and forecasting of potential activity. Yet fundamental questions regarding the source of nuclides in geothermal waters and the time scale of water-rock interaction in the Yellowstone hydrothermal system remain unresolved. Lacking information on the time scale of subsurface hydrothermal fluid circulation, there exists an indeterminate lag time between observed changes in the geochemistry or activity of hydrothermal features at the surface and changes in hydrothermal and volcanic processes at depth. Additionally, the chemistry of the Yellowstone system can serve as a rough natural analogue for mid-ocean ridge hydrothermal systems where direct geochemical sampling from would be difficult or cost prohibitive. Understanding hydrothermal processes in Yellowstone is important because hydrothermal processes are associated worldwide with epithermal ore deposits of gold, copper, lead, zinc, and other economically valuable minerals.

To constrain the time scale of processes in the active and dynamic Yellowstone hydrothermal system requires the use of chronometers capable of measuring current to recent processes. One such chronometer is the uranium-thorium series of radioisotopes (Figure 1). Radon and radium isotopes are particularly well suited to the study of current to recent processes in Yellowstone, because of the wide range in the time scale of their half-lives and their different behavior in solution.

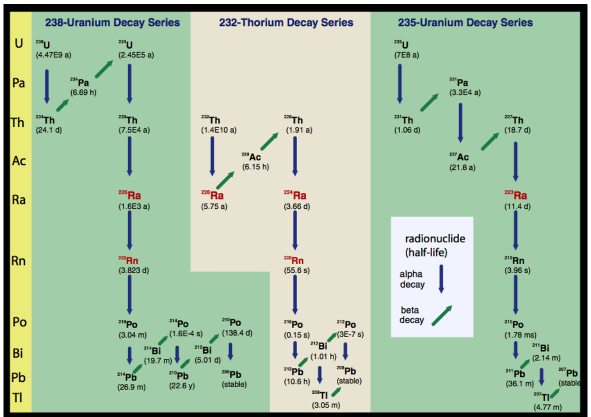

Figure 1. The decay series of ^{238}U, ^{232}Th, and ^{235}U. The half-life of each isotope is given under the symbol. Isotopes measured in this study are shown in red.

Studies of radium isotopes in YNP have previously explored regional differences in hydrothermal geochemistry (Clark and Turekian, 1990; Sturchio et al., 1993), the time scale of water-rock interactions in thermal aquifers (Clark and Turekian, 1990), the aquifer properties controlling isotopic composition and ratios (Sturchio et al., 1989; Sturchio et al., 1993), and near surface groundwater flow velocities (Sturchio et al., 1993). Some reconnaissance data on radon in thermal areas has been collected (Jaworowski et al. 1996). However, to date the spatial and temporal distribution of ^{222}Rn in areas of thermal activity has not been studied in detail. Neither has any study of its sister isotope ^{220}Rn (thoron) been carried out.

The purpose of this study is to measure radon, radium, chloride, and CO_2 in water samples from hot springs and in soil gas. The isotopic ratios of radon and radium will be used in conjunction with measurements of magmatic volatiles (chlorine and CO_2) to estimate the relative contribution of the magmatic source vs. non-magmatic sources, i.e., soil and aquifer rocks. The measured activities of radium and radon, based on their half-lives, will be used to assess relative time scales of hydrothermal circulation in different areas.

STUDY AREA

The Yellowstone Plateau volcanic field is the world's largest and most concentrated area of continental hydrothermal activity (Figure 2). Over the past 2.2 million years, the region has experienced three explosive caldera forming eruptions, the most recent of which expelled >1000 km^3 of rhyolitic magma about 640,000 years ago (Christiansen, 2001). Two active resurgent domes exist inside the caldera boundary. Heat flux from the magma system below this still active volcanic field is maintained by the circulation of hydrothermal fluid overlying the magma chamber. Heat and volatile flux from the hydrothermal system can be estimated by monitoring the composition and volume of emitted hydrothermal fluid.

There are three principal types of hydrothermal fluid in Yellowstone, classified according to their pH and major anion composition: neutral-chloride, acid-sulfate, and calcium-bicarbonate sulfate (Fournier, 1989). Neutral-chloride fluids generally surface at lower elevations (Lowenstern and Hurwitz, 2008), and they are commonly associated with areas of major geyser activity (e.g., Old Faithful). Neutral chloride fluids contain high concentrations of chloride, alkalis, and silica, but low concentrations of sulfate and alkaline earths. Acid-sulfate fluids generally surface at higher elevations, and are commonly associated with mudpots and fumarolic activity. These fluids form when geothermal steam (containing H_2S) condenses into shallow, oxygenated meteoric water. The H_2S is oxidized to sulfate, lowering the pH of the solution and producing a sulfate-rich fluid. Calcium-bicarbonate-sulfate type waters have high concentrations of Ca^{2+}, HCO_3^-, and SO_4^{2-}. These waters generally have high TDS compared to other Yellowstone waters. They are generated by dissolution of sedimentary rocks (notably limestone and $CaSO_4$ minerals) at depth, typically at lower temperatures compared with other hydrothermal fluids in Yellowstone. Calcium-bicarbonate-sulfate waters precipitate travertine at the surface. Such waters may occur in many areas in Yellowstone, but they are most common in the area of Mammoth Hot Springs.

Surficial hydrothermal discharge in Yellowstone occurs primarily from areas within or around the 640,000 year old caldera. There is a major area of activity in the valley of the Firehole River, including the Upper, Lower, Midway, and Lone Star Geyser Basins. The Firehole River carves its path between rhyolite lava flows and also lies near the ring-fracture zone of a resurgent dome. Another major area of activity is Norris Geyser Basin, which lies just outside the caldera rim at the intersection of two fault zones. A concentration of earthquake activity extends west from Norris to Hebgen Lake (site of a 7.5 magnitude earthquake in 1959), and an alignment of normal faults and fractures termed the Norris-Mammoth Corridor extends north from Norris to Mammoth Hot Springs. The Norris-Mammoth Corridor is also a locus of hydrothermal activity.

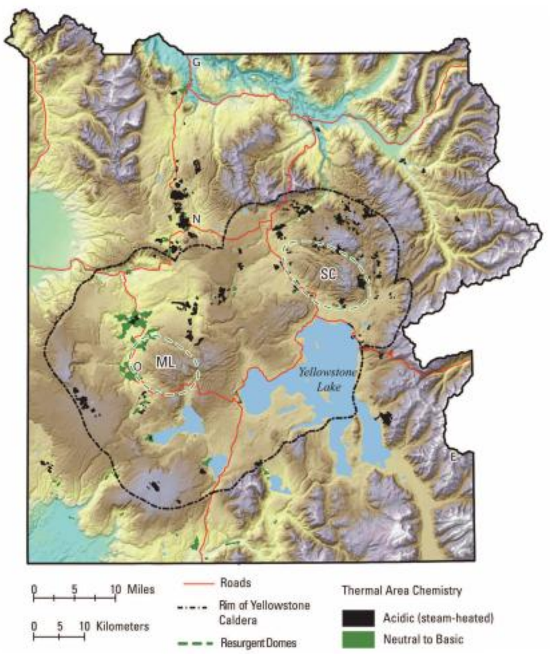

Figure 2. Yellowstone National Park's surficial geography and major areas of hydrothermal activity. Modified from Lowenstern and Hurwitz (2008).

Radiogenic nuclides in Yellowstone's hydrothermal fluids may be sourced from decay of uranium and thorium in magma, aquifer rocks, or soils. Secular equilibrium is likely to exist in the magma reservoir between ^{238}U and ^{226}Ra, and between ^{232}Th and ^{224}Ra. U, Th, Ra, and/or Rn escape from the magma dissolved in gases and brines, and proceed to interact with aquifer rocks on the way to the surface. Quaternary volcanic rocks overlying the magma chamber range from ~600,000 to ~70,000 years in age and commonly display disequilibrium in the upper portion of the U and Th decay chains (Vasquez and Reid, 2002). Mesozoic sedimentary rocks are the principle aquifers north of the caldera. These rocks generally contain little ^{232}Th (Clark and Turekian, 1990; Sturchio et al., 1993). On the east side of Yellowstone, the rocks of the ~50 Ma Absaroka Volcanic Supergroup are present.

The locations sampled in this study were thermal springs (Appendix Table 1), rivers (Appendix Table 2), fumaroles (Appendix Table 3), and areas of bedrock exposure for collection of rock samples (Appendix Table 4). Sites were selected based on three criteria: 1) Water-chemistry type and geographic location. Sites were selected to represent neutral-chloride, acid-sulfate, and calcium-bicarbonate-sulfate water types, and to provide comparison between different major thermal areas; (2) Ease of access. Sample sites needed to be accessible by a day hike, but remote enough to avoid crowds of park visitors; (3) anticipated geochemistry. An effort was made to sample some springs for which previous data on radionuclides exists. Water samples were collected and gas measurements made in the field between May 24th, 2010 and September 24th, 2010.

Measurements of CO_2 efflux and radon activity in gas were made at each locality. Some springs were sampled several times to determine the seasonal variability in radionuclide activity. In total, 25 gas measurements were taken, and 23 springs were sampled. Due to equipment failure or other logistical difficulty, it was not always possible to measure all parameters at each site.

✦ METHODS

Radon

Radon-222 and ^{220}Rn were measured in the field with the Durridge RAD7, RAD AQUA, and RAD H_2O (http://www.durridge.com). The instruments were calibrated by Durridge prior to the field season. The RAD7 is a portable, battery powered radon-in-air monitor, which uses a solid-state alpha detector to convert alpha radiation to an electrical signal. Based on the energy of the signal, the detector discriminates between the decays of the different daughter products. The RAD H_2O is an attachment that bubbles gas through a small sample of water and intakes the gas into the RAD7 for detection of radon. Because of the time delay in collecting a sample and setting up the sampling apparatus, it is usually impossible to measure ^{220}Rn with the RAD H_2O. The RAD AQUA is a continuous radon-in-water monitor. Water passes continuously through the exchanger in the RAD AQUA, and air flows in a closed loop through the exchanger and through the RAD7. This allows radon in water to come into equilibrium with the radon in the air, and the RAD AQUA (detection limit below 1 pCi/L), but the RAD H_2O requires only a 250 mL water sample, whereas the RAD AQUA requires continuous flow. The most appropriate method for analysis of radon and thoron in water was chosen on a site-to-site basis. Generally, the RAD AQUA was used if possible, due to its lower detection limit, higher degree of accuracy, and its ability to detect ^{220}Rn.

Radium

Radium activities in water were measured following the method of Moore and Arnold (1996) and Moore (2008). Radium-228, ^{226}Ra, ^{224}Ra, and ^{223}Ra were pre-concentrated on manganese fibers in the field. Ten to 21 L of water were pumped from the source through a plastic column filled with acrylic fibers impregnated with manganese oxide. The water was collected in a reservoir so a volume measurement could be made, and then returned to the channel. The activity of ^{223}Ra and ^{224}Ra on the Mn fibers was measured within 3 days in a field laboratory with a radium delayed coincidence counter (or RaDeCC™). The RaDeCC is a large Lucas Cell, which uses a pump and helium carrier gas to distribute built-up ^{220}Rn and ^{219}Rn throughout an air loop. The loop is sealed for 5 minutes to allow daughter ingrowth, and counted for approximately three hours with delayed coincidence counting software. The system was calibrated with a standard solution of ^{228}Ra. The RaDeCC method has very low error (±10%), and an analytical detection limit of approximately 0.0005 dpm/L (Moore, 2008).

The activity of ^{228}Ra on the Mn fibers was determined subsequently by repeated counts on the RaDeCC to monitor the ingrowth curve of its great-granddaughter, ^{224}Ra. Radium-224 quickly establishes secular equilibrium with its parent ^{228}Th, which is in transient equilibrium with ^{228}Ra. The Bateman Equation is fit to the data and used to extrapolate to the initial activity of ^{228}Ra (Figure 3). For this analysis, each Mn fiber sample was counted at least 3 times over a period of approximately 6 six months. For comparison, six selected samples were shipped to Woods Hole Oceanographic Institution where the activity of ^{228}Ra was also determined by gamma counting of its direct daughter, ^{228}Ac.

The activity of ^{226}Ra on the Mn fibers was measured by counting with a RAD7 (Kim et al., 2001; Dimova et al., 2007). The Mn fibers were sealed in a column for ≥20 days to allow ingrowth of ^{222}Rn, and the column was then attached to a recirculating closed-air loop connected to the RAD7. Each sample was counted for at least 3 hours, and only the last 2 hours of counting data was used to calculate ^{226}Ra activity. The RAD7 counts the decays of ^{218}Po, the direct daughter of ^{222}Rn, which establishes secular equilibrium with ^{222}Rn after about 15 minutes. The RAD7 was calibrated with a ^{226}Ra standard solution.

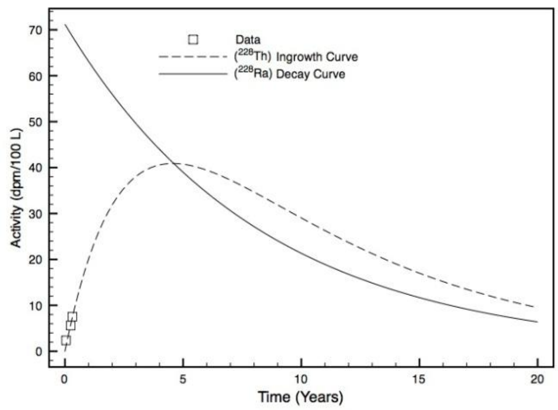

Figure 3. Example of ^{228}Th ingrowth data obtained by measuring ^{224}Ra on the RaDeCC, and the equations fit to estimate the initial activity of ^{228}Ra. Data shown is for the sample from Beryl Spring on 9/22/2010.

CO_2 Flux Measurements

Carbon dioxide effluxes in soil and fumarole emissions were measured using the accumulation chamber method (Chiodini et al., 1998). A cylindrical chamber with an open bottom was placed on the ground surface and the rate of increase in the CO_2 concentration inside the chamber is measured. The chamber mixes the gas with an internal fan and is connected with a portable non-dispersive infrared spectrophotometer. The change in concentration over the time of the measurement is proportional to the CO_2 efflux.

CO_2 flux from the surface of hot springs was measured by a modified version of the accumulation chamber method. In this case the cylindrical chamber was a 1-liter HDPE bottle attached to an extension pole used to place the bottle near the center of the spring while the operator controlled it safely from the edge. An outlet tube at the top of the bottle was connected to the portable detector, while a return tube was run from the detector outlet to the side of the bottle near the base (just above the water surface when sampling). This system suffers from the drawback that there is no internal fan to ensure mixing, but the placement of the outlet and return tubes on the bottle attempts to promote the most mixing possible.

Other Geochemical Parameters

On-site geochemical and environmental parameters were measured with a YSI Professional Plus multi-meter (http://www.ysi.com/). The multi-meter was configured to measure pressure, temperature, dissolved oxygen, pH, oxidation-reduction potential, and specific conductance. The meter was calibrated prior the start of fieldwork and approximately every two weeks throughout the field season.

From each spring sampled, two 50-mL water samples were collected for chemical analysis. The water was collected from its source with a 60-mL HDPE syringe and filtered through a 0.45-µm syringe filter into 60-mL LDPE bottles. One sample was acidified with 1% v/v of ultra-high purity nitric acid for analysis of cations. No chemical preservative was added to the second sample, which was used to determine anion concentrations. The samples were stored on ice or in a refrigerator and were analyzed at the US Geological Survey trace metal laboratory in Boulder, Colorado. Concentrations of Br, Cl, F, and SO_4 were measured by ion chromatography and cations were measured by inductively coupled plasma-optical emission spectrometry using the methods described in Ball et al. (2010). Alkalinity was determined by titration with H_2SO_4 to the HCO_3 endpoint (Barringer and Johnsson, 1996). In the case where our research group was collaborating in the field with the USGS-Boulder research group and sampling the same springs, we used their chemical data. The methods used by the by the USGS-Boulder group are detailed in Ball et al. (2010).

Data on helium isotopes in gas emissions was provided by Jacob Lowenstern (Bergfeld et al, in press). In some cases, radionuclide activities measured at several discrete locations were averaged together to give a single value for comparison to the helium isotope data set.

✦ PRELIMINARY RESULTS

Spring Chemistry

Geochemical and environmental parameters measured on-site are summarized in Appendix Table 5. Basic water chemistry of thermal springs determined by laboratory analysis is summarized in Appendix Table 6. Charge balances were calculated using WATEQ4F by the USGS trace metal lab in Boulder, CO. Charge was balanced within +/- 5% for all samples except Soda Butte 5/30 and Narrow Gauge Terrace 9/24, where anion charge appeared anomalously low. The pH of the sampled springs ranged from 2.36 to 9.28. Chloride ranged from 55 to 792 mg/L, [SO_4^{2-}] ranged from 15 to 607 mg/L, (^{223}Ra) ranged from 0.0001 to 3.13 dpm/L, (^{224}Ra) ranged from 0.0053 to 21.47 dpm/L, (^{226}Ra) ranged from 0.037 to 1.39 dpm/L, and (^{228}Ra) ranged from 0.05 to 20.9 dpm/L.

The springs sampled divide into three major groups based on location and water-type. Springs from Norris Geyser Basin and nearby Beryl Spring have highly variable pH and chloride concentration but are generally high in sulfate and low in fluoride. Generally these springs are best classified as acid-sulfate water type. Springs from the Lower Geyser Basin and nearby Rabbit Creek Hot Springs can be classified as neutral-chloride type waters. They are generally alkaline, high in chloride and fluoride, and low in sulfate. The springs from Mammoth Hot Springs are calcium-bicarbonate-sulfate water type. They are neutral to alkaline with high concentrations of sulfate, bicarbonate, and alkali earths.

The most significant correlations in the chemistry of spring water were between radium and pH (Spearman's Correlation, $\rho = -0.609(21)$, p (two-tailed) $< .01$), radium and ORP (Spearman's Correlation, $\rho = 0.712(21)$, p (two-tailed) $< .01$), radium and DO (Spearman's Correlation, $\rho = 0.714(13)$, p (two-tailed) $< .01$), radium and barium (Spearman's Correlation, $\rho = 0.621(21)$, p (two-tailed) $< .01$), and radium and calcium (Spearman's Correlation, $\rho = 0.849(21)$, p (two-tailed) $< .01$). Important observations included that radium activity in springs was positively correlated with many major dissolved ions including Br, SO_4, Cl, B, Ba, Ca, Fe, K, Li, Mg, Mn, Mo, and Sr, and was also controlled by the Eh and pH of the spring water.

Radon

Measurements of radon isotopes in gas emissions from fumaroles and CO_2 fluxes determined by the accumulation chamber method are given in Appendix Table 7. Radon activities measured in thermal springs are given in Appendix Table 8. Relevant activity ratios and CO_2 fluxes determined by the modified accumulation chamber method are listed in Appendix Table 9. Combining all gas and water measurements, radon activities ranged from 0.1 to 1173 pCi/L, thoron activities ranged from 0.2 to 300 pCi/L, and CO_2 fluxes ranged from 1.92 to 3909 g m^{-2} d^{-1}.

Radon activity in spring water showed a weak inverse relationship with spring temperature (not statistically significant). Radon activity was positively correlated with CO_2 flux, Figure 4F, Spearman's Correlation, ρ = 0.364(42), *p* (two-tailed) < .05), while Thoron activity increased with CO_2 flux up to about 100 g m-2 d-1 and decreased with increasing CO^2 flux thereafter (Figure 4E). ($^{220}Rn/^{222}Rn$) and CO^2 flux from springs and gas vents showed a weak inverse correlation (Figure 5, Spearman's Correlation, ρ = -0.344[40], *p* [two-tailed] < .05). In general, gas vents had higher ($^{220}Rn/^{222}Rn$) than springs (Figure 5C). Mean ($^{220}Rn/^{222}Rn$) from gas vents was 2.4, while mean ($^{220}Rn/^{222}Rn$) from springs was 0.69.

In a limited dataset, neither radon, thoron, nor ($^{220}Rn/^{222}Rn$) showed any relationship with ($^{3}He/^{4}He$) values reported for thermal features by the USGS (Figure 6). Neither did thoron, radon, nor ($^{220}Rn/^{222}Rn$) show any relationship with chloride in spring water (Figure 7).

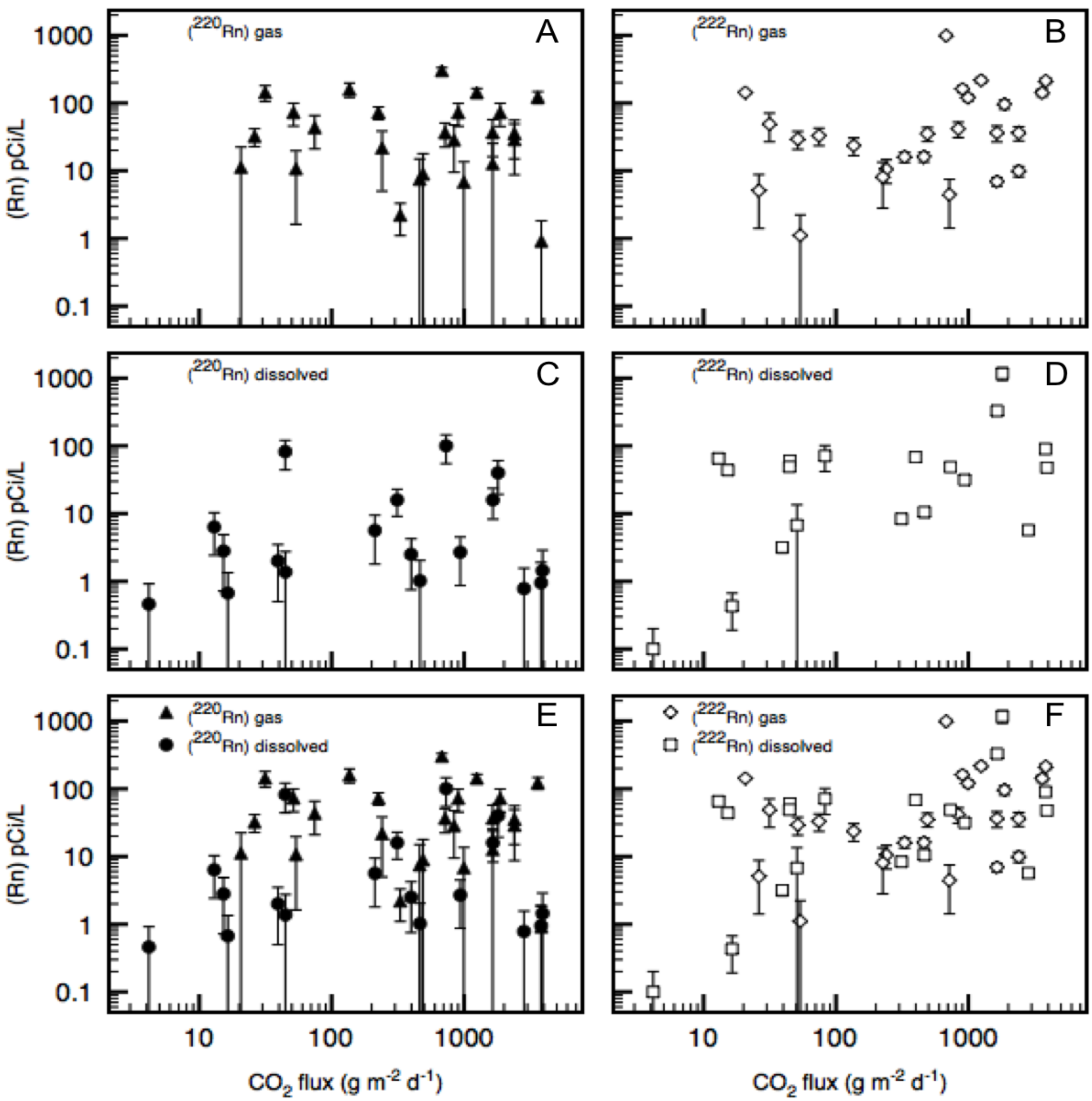

Figure 4. Data on ^{222}Rn and ^{220}Rn in hydrothermal fluids in Yellowstone. (^{220}Rn) appears to increase with CO_2 flux to about 100 g m^{-2} d^{-1}, then decrease with higher CO_2 fluxes (E). (^{222}Rn) shows a weak positive correlation for all values of CO_2 flux (F).

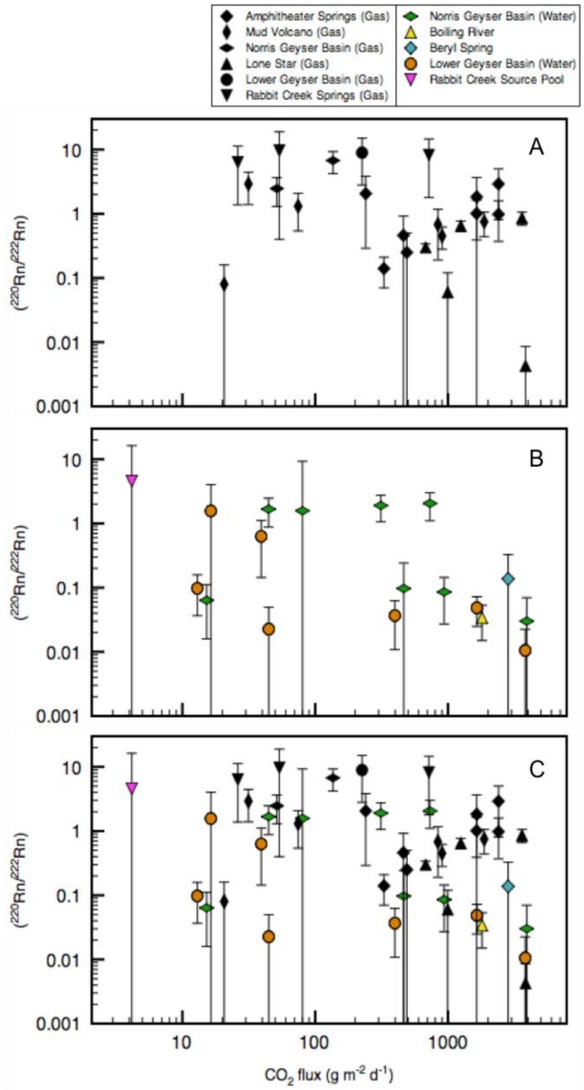

Figure 5. Weak inverse correlation between ($^{220}Rn/^{222}Rn$) and CO_2 flux in from gas vents (A), thermal springs (B), as vents and springs (C).

Radium

Radium activities measured in thermal springs are given in Appendix Table 8. Relevant activity ratios are listed in Appendix Table 9. Radium concentration in springs was positively correlated with many major dissolved ions including Br, SO_4, Cl, B, Ba, Ca, Fe, K, Li, Mg, Mn, Mo, and Sr, and was also significantly correlated wtih the Eh, Spearman's Correlation, $\rho = 0.712(21)$, p (two-tailed) $< .01$) and pH, Spearman's Correlation, $\rho = -0.609(21)$, p (two-tailed) $< .01$) of the spring water. Radium activity was inversely correlated with fluoride concentration. ((Spearman's Correlation, $\rho = -0.644(20)$, p (two-tailed) $< .01$)).

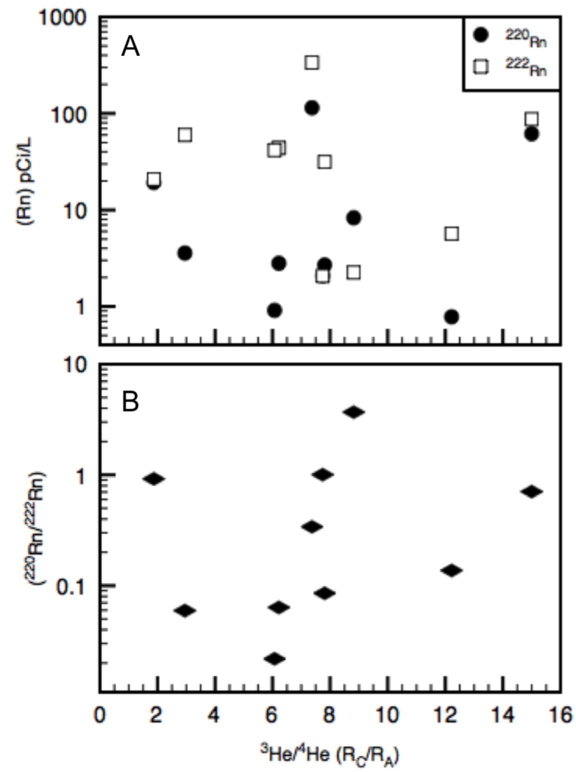

Figure 6. Radon isotopes show no relationship with helium isotope ratios in Yellowstone. Data on ($^3He/^4He$) from Bergfeld et al., in press. The measurements of radon and helium isotopes were not concurrent and in some cases represent an average of available data points in a similar area.

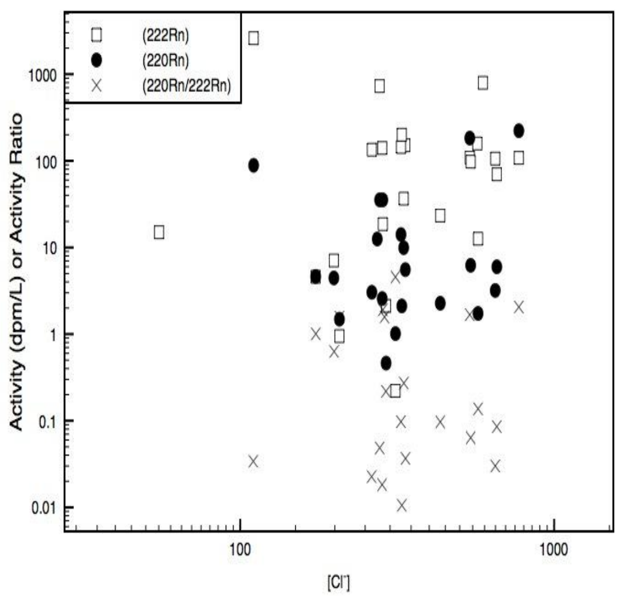

Figure 7. Thoron, radon, and ($^{220}Rn/^{222}Rn$) dissolved in spring water showed no relationship with chloride concentration.

Radium-223 ranged from 0.00008 to 3.13 dpm/L, ^{224}Ra ranged from 0.0053 to 21.47 dpm/L, ^{226}Ra ranged from 0.037 to 1.39 dpm/L, and ^{228}Ra ranged from 0.05 to 20.9 dpm/L. In general, ^{228}Ra is present in the greatest activity in thermal springs in Yellowstone, followed by ^{224}Ra, ^{226}Ra, and finally ^{223}Ra. No radium isotope showed a significant correlation with CO_2 flux, (^{3}He/^{4}He), or chloride, but all radium isotopes were significantly correlated with barium concentration in spring water (Figure 8).

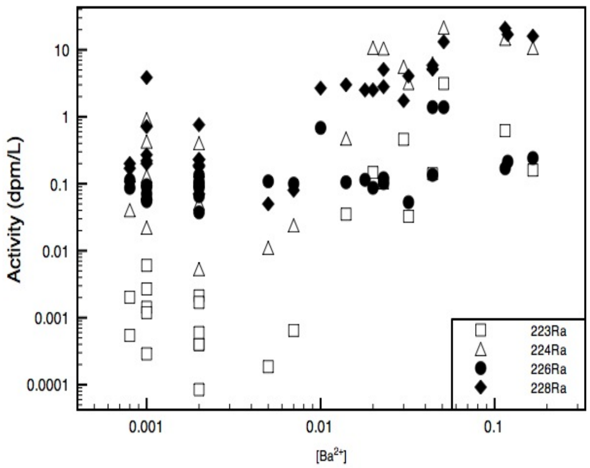

Figure 8. All radium isotopes (and total radium) showed a significant positive correlation with barium concentration in spring water.

^{223}Ra and ^{224}Ra

(^{224}Ra/^{223}Ra) ranged from 6.86 to 298.47. (^{224}Ra/^{223}Ra) showed a weak inverse correlation with CO_2 flux (not statistically significant, Figure 9A). This correlation was strong for the neutral-chloride springs of the Lower Geyser Basin and Rabbit Creek Hot Springs, but the other springs showed no relationship between (^{224}Ra/^{223}Ra) and CO_2 flux. (^{224}Ra/^{223}Ra) showed no relationship with [Cl$^-$] or (^{3}He/^{4}He) (Figures 10A, 11).

^{224}Ra and ^{228}Ra

(^{224}Ra/^{228}Ra) ranged from 0.076 to 4.26. (^{224}Ra/^{228}Ra) was often greater than 1 for the springs from Norris Geyser Basin and Mammoth Hot Springs (mean = 1.60), but was usually less than 1 for the Lower Geyser Basin and Rabbit Creek Hot Springs (mean = 0.37). (^{224}Ra/^{228}Ra) showed no significant relationship with CO_2 flux, [Cl$^-$], or (^{3}He/^{4}He) (Figures 9B, 10B, 11).

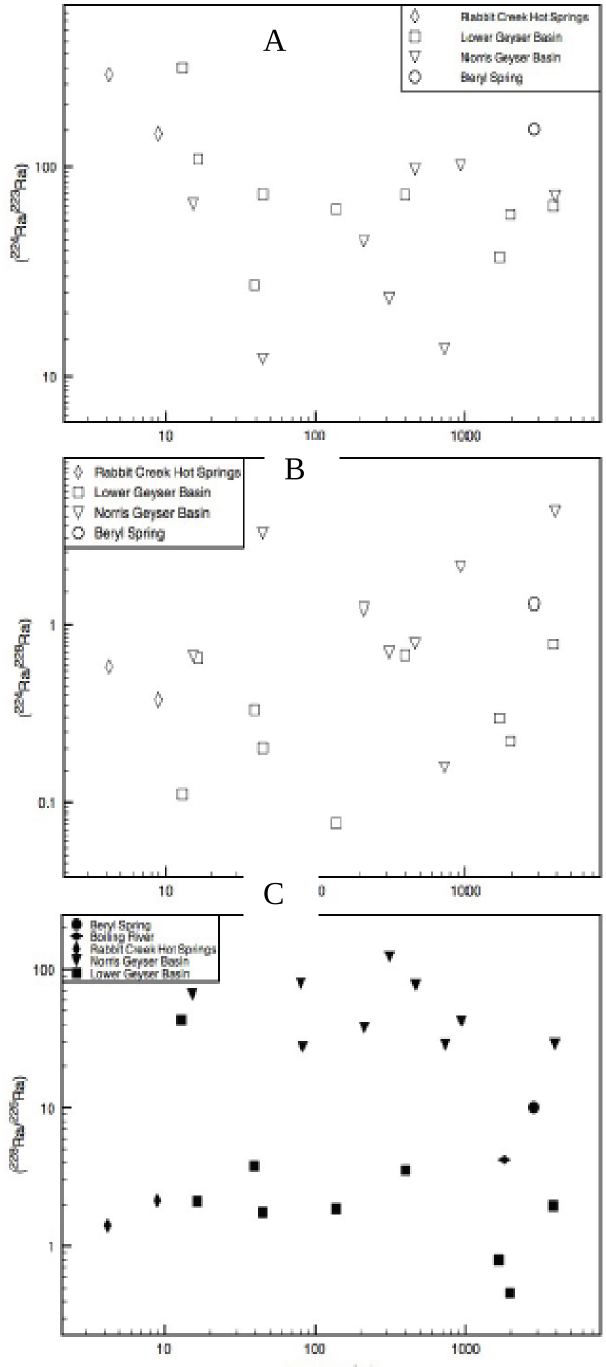

Figure 9. (^{224}Ra/^{223}Ra) in thermal spring water was negatively correlated with CO_2 flux (A), while (^{224}Ra/^{228}Ra) and (^{228}Ra/^{226}Ra) showed no relationship with CO_2 flux (B,C). The correlation between (^{224}Ra/^{223}Ra) and CO_2 flux (A) was strong for the springs of the the Lower Geyser Basin and Rabbit Creek Hot Springs, while (^{224}Ra/^{223}Ra) from springs in other areas did not show a strong relationship with CO_2 flux.

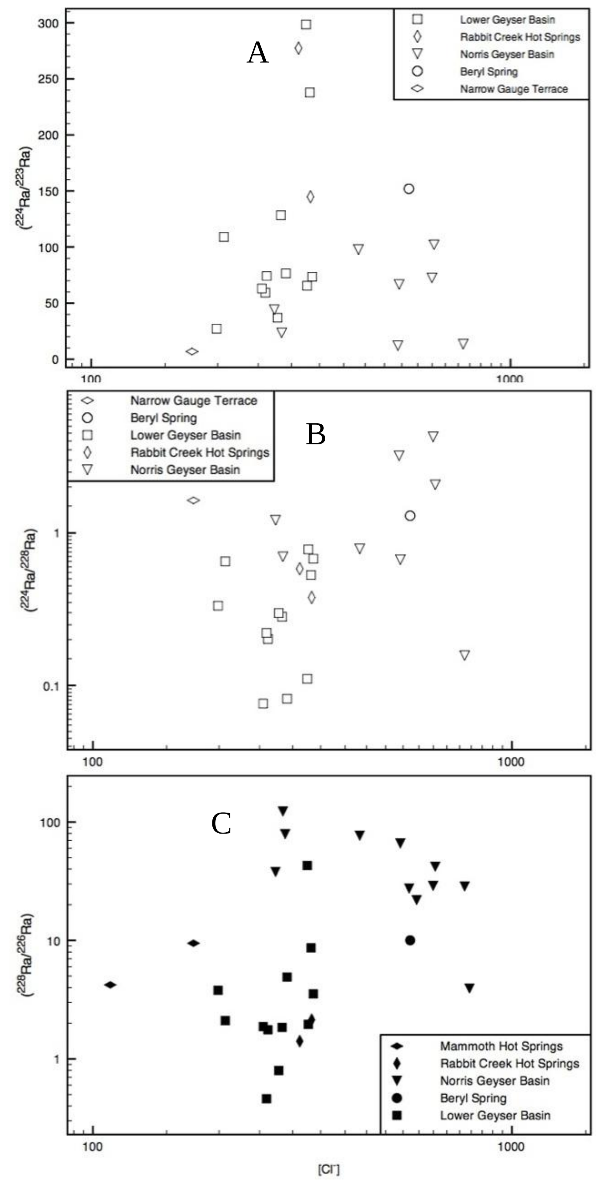

Figure 10. There were no significant relationships between ($^{224}Ra/^{223}Ra$) and [Cl^-] (A), or ($^{224}Ra/^{228}Ra$) and [Cl^-] (B). The acid-sulfate springs in the Norris Geyser Basin and Beryl Spring showed a negative correlation between ($^{228}Ra/^{226}Ra$) and [Cl^-], but springs from other areas showed no relationship between ($^{228}Ra/^{226}Ra$) and [Cl^-] (C).

^{226}Ra and ^{228}Ra

($^{228}Ra/^{226}Ra$) ranged from 0.46 to 122.82. ($^{228}Ra/^{226}Ra$) was often greater than 10 for the springs from Norris Geyser Basin and Mammoth Hot Springs (mean = 39.92), but was usually less than 10 for the Lower Geyser Basin and Rabbit Creek Hot Springs (mean = 5.58). ($^{228}Ra/^{226}Ra$) was inversely correlated with [Cl^-] for the acid-sulfate springs of the Norris Geyser Basin and Beryl Spring (Pearson's Correlation, r = -0.717(9), *p* (two-tailed) < .05 but the other springs showed no relationship between ($^{228}Ra/^{226}Ra$) and [Cl^-]. ($^{228}Ra/^{226}Ra$) showed no significant relationship with CO_2 flux (Figure 9C). A small dataset (5 data points) suggests that ($^{228}Ra/^{226}Ra$) may have been inversely correlated with ($^3He/^4He$), although the sample size was too small to be statistically significant (Figure 11).

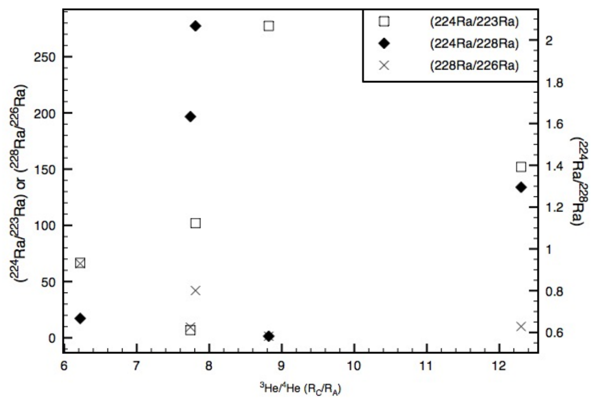

Figure 11. In a very small dataset, ($^{224}Ra/^{223}Ra$) and (224/^{228}Ra) showed no relationship to ($^3He/^4He$). ($^{228}Ra/^{226}Ra$) showed a negative correlation with ($^3He/^4He$) (not statistically significant, due to small n). ($^3He/^4He$) data from Bergfeld et al., in press.

^{224}Ra and ^{222}Rn

($^{224}Ra/^{222}Rn$) ranged from 0.00003 to 0.78 (excluding Narrow Gauge Terrace, which had an outlier value of 4.68). ($^{224}Ra/^{222}Rn$) was inversely correlated with [Ba^{2+}/Cl^-] ((Spearman's Correlation, ρ = 0.535(18), *p* (two-tailed) < .05)).

✦ DISCUSSION

Radon and CO_2

There is a weak inverse relationship between ($^{220}Rn/^{222}Rn$) and CO_2 flux from thermal features (Figure 5). This is driven by a positive link between (^{222}Rn) and CO_2 flux (Figure 4F) and an apparent inverse correlation between (^{220}Rn) and CO_2 flux values above 100 g m^{-2} d^{-1} (Figure 4E). Although this correlation may be of some use in assessing the local depth of sourcing for hydrothermal fluids in different areas of Yellowstone, (^{220}Rn) and (^{222}Rn) will be strongly affected by variations in the ^{238}U and ^{232}Th content of local aquifer rocks. Simple flow velocity calculations show that if ^{222}Rn is sourced from magma 6 km below the surface (a likely depth from Lowenstern and Hurwitz, 2008), ^{222}Rn would need to move vertically at a velocity of 13 meters per hour to reach the surface before decaying to undetectable levels (5 half lives, 19.25 days). This figure is an order of magnitude higher that estimated near surface flow velocities in Yellowstone (Sturchio et al., 1993). Thus it is unlikely that any ^{222}Rn venting at the surface is sourced from magma in Yellowstone, and the utility of the radon isotope system for understanding magmatic processes is limited. This conclusion is supported by the observation that (^{220}Rn), (^{222}Rn), and (^{220}Rn/^{222}Rn) show no relationship with (^{3}He/^{4}He) isotope ratios (Figure 6). If (^{220}Rn/^{222}Rn) was strongly influenced by magmatic processes, one would expect an inverse correlation between between (^{220}Rn/^{222}Rn), which should be low in areas of intense magmatic degassing, and (^{3}He/^{4}He), which is higher in areas with a direct connection to the mantle.

If we accept that the inverse correlation between (^{220}Rn/^{222}Rn) and CO_2 flux is related to the age of the hydrothermal fluid, and hence its depth of sourcing, then the relative depths of sourcing can be assessed by examination of Figure 5. Areas of relatively deep fluid sourcing plot in the lower right of the figure, areas of relatively shallow fluid sourcing plot in the upper left, and areas of intermediate source depth plot in the center. By this analysis, Beryl Spring, Boiling River, and Lone Star Geyser Basin are areas where hydrothermal fluid sourcing is relatively deep. Rabbit Creek Hot Springs is an area where hydrothermal fluid sourcing is relatively shallow. Amphitheater Springs has an intermediate source depth. The Lower and Norris Geyser Basins show a wide range of depths including some areas with a shallow signature and some with a deep signature. This analysis should be interpreted with caution due to local heterogeneity and variations in gas flow velocity. It should also be noted that none of the interpretations made above holds when examining the relationship between (^{220}Rn/^{222}Rn) and (^{3}He/^{4}He) in Figure 6B.

Generally, (^{220}Rn/^{222}Rn) in fumarolic gas was slightly greater (mean = 2.4) than (^{220}Rn/^{222}Rn) dissolved in spring water (mean = 0.69, Figure 5C). In the context of the two-component mixing model, the radon in the gas has a younger isotopic signature than the radon dissolved in water. Based on field observations of fluid discharge velocity, it is possible that the gaseous fluids discharging from fumaroles move at greater velocity than the liquid fluids discharging from springs and this accounts for the observed difference in isotopic signature. Alternatively, it is also possible that the method used for sampling the short-lived (^{220}Rn) in spring water consistently underestimates the activity due to rapid decay between the sampling point and the detector. If such a sampling bias exists, there may be no consistent difference between (^{220}Rn/^{222}Rn) in hydrothermal waters and gases.

^{224}Ra, ^{222}Rn, and Recoil Supply Efficiency

Krishnaswami et al. (1982) proposed that the activity of ^{222}Rn in groundwater could be used to estimate the recoil supply of other nuclides. Because radon is a noble gas and chemically inert, the steady-state activity (achieved after ~20 days) of radon in the aquifer will be equal to its recoil supply rate. The recoil supply rate of other nuclides can then be related to radon's supply rate:

$$F_i=\varepsilon*F_r*Q_i/Q_r$$

where,

F_r is the recoil supply rate of radon (atoms min^{-1} l^{-1})

F_i is the recoil supply rate of nuclide i (atoms min^{-1} l^{-1})

Q_r is the production rate of radon in aquifer solids (atoms min^{-1} l^{-1})

Q_i is the production rate of nuclide i in aquifer solids (atoms min^{-1} l^{-1})

ε is the recoil supply efficiency of nuclide i relative to radon (dimensionless)

The term (Q_i/Q_r) is approximated by the (^{228}Ra/^{226}Ra) activity ratio in aquifer rocks. Assuming secular equilibrium in Yellowstone's aquifer rocks, this is equal to the (^{232}Th/^{238}U) ratio, which in Yellowstone's tuffs and rhyolites is generally greater than 1 and less than 2 (Clark and Turekian, 1990, Sturchio et al., 1993). An average value of 1.3 is used for these calculations.

Krishnaswami et al. (1982) proposed that the value of ε is determined by the position of the to the nuclide within the decay chain and the adsorptive properties of its parent. Kadko and Butterfield (1998) used ^{224}Ra and ^{222}Rn to estimate recoil supply efficiencies of radium isotopes at the Juan de Fuca Ridge hydrothermal system, and found that the ^{224}Ra supply rate is 20% of what it would be expected to be based on ^{222}Rn (effectively, ε=0.2). In an aquifer, ^{224}Ra is produced by alpha decay of ^{228}Th ($T_{1/2}$ = 1.91 yr), which is insoluble under most conditions. Assuming there is little ^{228}Th in solution, the ^{224}Ra activity in solution is likely to be equal to its recoil supply rate.

Activities of ^{222}Rn and ^{224}Ra in hot spring water from Yellowstone National Park do not show a positive correlation as would be expected if ε and (Q_i/Q_r) were uniform throughout the aquifer (Figure

12). This is most likely because there is significant variance in the ($^{228}Ra/^{226}Ra$) ratio in the aquifer solids (Sturchio et al. 1993). Nevertheless, nearly all the samples collected in this study lie above the expected curve if ε=0.897 as calculated by Krishnaswami et al. (1982) for Connecticut groundwater. The average ($^{224}Ra/^{222}Rn$) ratio for all samples collected is 0.39, implying that ε=0.3. However, one value of the ($^{224}Ra/^{222}Rn$) ratio from Narrow Gauge Terrace is anomalously large (5.5, all other values <1.07). This is probably because the spring geometry at Narrow Gauge makes it impossible to sample the vent directly. A side pool was sampled that had likely degassed radon to the atmosphere while retaining its radium. Excluding this value from the average gives ($^{224}Ra/^{222}Rn$) = 0.1226, which gives ε=0.09. A range of ε values from 0.3 to 0.09 is comparable to the value of 0.2 observed by Kadko and Butterfield (1998) at the Juan de Fuca Ridge.

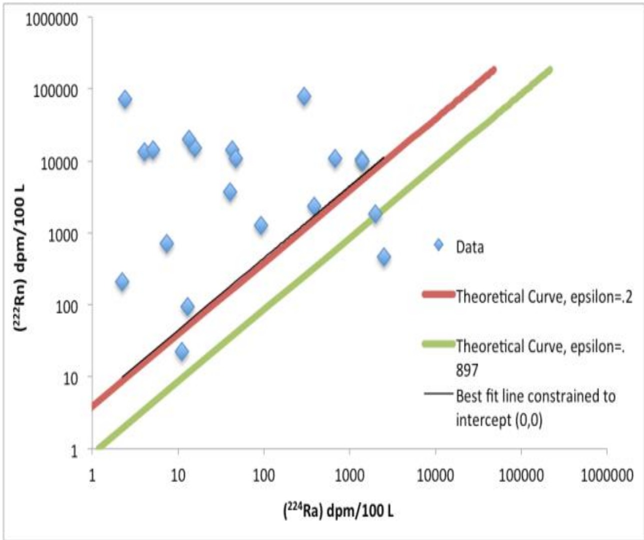

Figure 12. Activities of ^{222}Rn and ^{224}Ra in hot spring water. Curves are plotted showing the expected relationship between ^{222}Rn recoil supply and ^{224}Ra recoil supply assuming a ($^{228}Ra/^{226}Ra$) value of 1.3 in the aquifer rocks. The lower curve is what would be expected if ε=0.897 as calculated by Krishnaswami et al. (1982). The higher curve is if ε=0.2 as found by Kadko and Butterfield (1998). ε=2 produces a line in better agreement with the best fit line, which is constrained to intercept the origin.

✦ CONCLUSIONS

The relationship between ($^{220}Rn/^{222}Rn$) and CO2 flux is statistically significant, but it is not strong, nor is it confirmed by any other isotope system, nor any other proxy of magmatic components, such as chloride concentration or ($^{3}He/^{4}He$) ratios. Our interpretation is that gas transport time from magma to surface in Yellowstone is greater than 20 days, such that no (^{222}Rn) or (^{220}Rn) venting to the surface is sourced directly from magma.

Gas vents, on average, are enriched in short lived (^{220}Rn) relative to spring water which is more enriched in the longer lived (^{222}Rn). This could possibly be due to greater fluid discharge velocity in gas vents relative to springs.

Neutral chloride springs in the Lower Geyser Basin and Rabbit Creek Hot Springs have isotopically old water that is enriched in the longer lived isotopes of radium, compared the to springs of Norris Geyser Basin and Mammoth Hot Springs which show relative enrichment of the shorter-lived radium isotopes.

Mineral (barite, in particular) precipitation may be a strong control on the amount of radium in solution in any given spring, as evidenced by strong correlations between the activity of all radium isotopes and [Ba2+] in spring water, and a correlation between ($^{224}Ra/^{222}Rn$) and [Ba^{2+}/Cl^{-}]. This removal of ^{224}Ra by precipitation (or other process such as sorption) results in a very low recoil supply efficiency for ^{224}Ra (and presumably all other radium isotopes) relative to ^{222}Rn. A reasonable efficiency is about 20%.

✦ ACKNOWLEDGEMENTS

In addition to support from the UW-NPS Research Station, this project has received key funding from the Department of Geology at the University of Wyoming, and the United States Department of Energy. The authors gratefully thank Kirk Nordstrom and Blaine McCleskey of the USGS, and the rest of their research group, for providing assistance and guidance in the field and their analysis of water samples. The study was aided by insightful guidance and input from Jacob Lowenstern of the USGS, Hank Heasler and Cheryl Jaworowski of NPS, and Matt Charette of Woods Hole Oceanographic Institution. We also wish to thank Hank Heasler, Cheryl Jaworowski, and Christie Hendrix for their help and cooperation in the use of NPS facilities, and Paul Henderson of WHOI for his work in gamma counting samples for this study. The authors are very grateful to all those individuals who assisted with fieldwork, including Allison Pluda, Tim Matthews, Chris Waters, Virginia Marcon, and Salvo Giammanco.

✦ LITERATURE CITED

Ball JW, McCleskey RB, Nordstrom DK. 2010, Water-chemistry data for selected springs, geysers, and streams in Yellowstone National Park, Wyoming, 2006-2008: U.S. Geological Survey Open-File Report 2010-1192, 109p. [http://pubs.usgs.gov/of/2010/1192/]

Barringer JL, Johnsson, PA. 1996. Theoretical considerations and a simple method for measuring alkalinity and acidity in low-pH waters by Gran titration. U.S. Geological Survey Water-Resources Investigations Report 89-4029, p. 36.

Bergfeld D, Lowenstern JB, Hunt AG, Shanks III WCP, Evans WC. in press. Gas and Isotope Chemistry of Thermal Features from Yellowstone National Park. U.S. Geological Survey Scientific Investigations Report 2010–XXXX.

Chiodini G, Cioni R, Guidi M, Raco B, Marini L. 1998. Soil CO_2 flux measurements in volcanic and geothermal areas, Applied Geochemistry, v. 13, p. 135–148.

Christiansen R. 2001. The Geology of Yellowstone National Park: The Quaternary and Pliocene Yellowstone Plateau Volcanic Field of Wyoming, Idaho, and Montana, USGS Professional Paper 729-G, 145p.

Clark JF, Turekian KK. 1990. Time scale of hydrothermal water-rock reactions in Yellowstone National Park based on radium isotopes and radon. Journal of Volcanology and Geothermal Research, v. 40, p. 169–180.

Dimova N, Burnett WC, Horwitz EP, Lane-Smith D, 2007. Automated measurement of ^{224}Ra and ^{226}Ra in water. Applied Radiation and Isotopes, v. 65, p. 428-434.

Fournier RO. 1989. Geochemistry and dynamics of the Yellowstone National Park hydrothermal system. Annual Reviews of Earth and Planetary Science, v. 17, p. 13-53.

Jaworowski C, Case JC, Larsen L, Reimer GM, Szarzi SL, Been JM, Crysdale B, Brown MA, Jacobs M, Martineau R, Wood J. 1996. Reconnaissance of radon in soil-gas and water in Yellowstone National Park. In: Wyoming Geological Association 47th Guidebook, pp. 324-358.

Kadko D, Butterfield DA. 1998. The relationship of hydrothermal fluid composition and crustal residence time to maturity of vent fields on the Juan de Fuca Ridge, Geochimica et Cosmochimica Acta, v. 62, p. 1521-1533.

Kim G, Burnett WC, Dulaivoa H, Swarzenski PW, Moore WS. 2001. Measurement of 224Ra and ^{226}Ra activities in natural waters using a radon-in-air monitor. Environmental Science and Technology, v. 35, p. 4680-4683.

Krishnaswami S, Graustein WC, Turekian KK, Dowd JF. 1982. Radium, Thorium and Radioactive Lead Isotopes in Groundwaters: Application to the in Situ Determination of Adsorption-Desorption Rate Constants and Retardation Factors, Water Resources Research, v. 18, p. 1633-1675.

Lowenstern JB, Hurwitz S. 2008. Monitoring a supervolcano in repose: heat and volatile flux at the Yellowstone Caldera. Elements, v. 4, p. 35–40.

Moore WS, Arnold R. 1996. Measurement of ^{223}Ra and ^{224}Ra in coastal waters using a delayed coincidence counter. Journal of Geophysical Research, v. 101, p. 1321-1329.

Moore WS. 2008. Fifteen years experience in measuring ^{224}Ra and ^{223}Ra by delayed-coincidence counting. Marine Chemistry, v. 109, p. 188-197.

Sturchio NC, Bohlke JK, Binz CM. 1989. Radium-thorium disequilibrium and zeolite-water ion exchange in a Yellowstone hydrothermal environment. Geochimica et Cosmochimica Acta, v. 53, p. 1025–1034.

Sturchio NC, Bohlke JK, Markun FJ. 1993. Radium isotope geochemistry of thermal waters, Yellowstone National Park, Wyoming, USA. Geochimica et Cosmochimica Acta, v. 57, p. 1203-1214.

Vasquez JA, Reid MR. 2002. Time scales of magma storage and differentiation of voluminous high-silica rhyolites at Yellowstone caldera, Wyoming. Contributions to Mineralogy and Petrology, v. 144, p. 274-285.

199

APPENDIX

Table 1. Locations and descriptions of sampled thermal springs.

Spring	Date	Time	Easting	Northing	Comment
Norris Geyser Basin					
Acid Spring	6/1/10	12:00	523031	4952617	Spring splashes to 0.5 m intermittently, durations >> intervals
Acid Spring	9/16/10	13:45	523031	4952617	"
Cinder Pool	9/20/10	11:20	522981	4953264	cloudy spring with black floating cinders
Cinder Pool	5/31/10	10:00	522968	4953267	"
Cojones	9/16/10	16:00	522807	4952852	Unnamed spring near Crystal Spring on White's 1975 Map
Cojones West	5/31/10	14:15	522809	4952858	"
Green Dragon Spring	9/21/10	17:15	523204	4951883	Cloudy spring in cavern, very hot
Medusa Spring	9/21/10	14:00	523036	4951767	Small clear spring on raised platform, runoff channels radiate in all directions
Perpetual Spouter	6/1/10	0:00	523028	4952623	Adjacent to Acid Spring
Perpetual Spouter	9/16/10	12:00	523028	4952626	"
Recess Spring	9/21/10	15:30	522969	4952194	Large clear spring, ~15 m diameter
Twin Bubblers West	9/21/10	10:00	523112	4953324	East of Cinder Pool; spring splashes vigorously from narrow vent spilling water onto platform
Lower and Midway Geyser Basins					
Azure Spring	7/27/10	14:00	513264	4934190	Clear, hot, blue spring
Bath Spring	7/27/10	15:30	513185	4934122	large, clear, hot, moderate bubbling
Imperial Geyser	7/31/10	15:00	509818	4930956	Sampled calm blue spring. Side vent to the east is a large, vigorous geyser. Small river of water discharge.
Mound Spring	8/6/10	14:10	511109	4934645	Clear, very hot, lots of bubbles, sits atop wide sloping mound
Mushroom Spring	7/28/10	13:15	516066	4931744	Low temperature, algae in spring vent, no bubbles
Octopus Spring	7/28/10	15:00	516059	4931221	Clear, hot, blue, deep spring
Ojo Caliente	7/27/10	11:45	512793	4934411	Clear, superheated, vigorous bubbling
Ojo Caliente	9/17/10	10:30	512816	4934422	"
Rabbit Creek Source Pool	8/4/10	11:00	514982	4929801	Very large spring (~20x40 m), small river of water discharge, no bubbling.
Lower and Midway Geyser Basins (continued)					
Scaffolding Pool	8/4/10	15:00	515034	4929633	clear, few bubbles, logs clutter the vent
Small black spring near Azure	7/27/10	14:30	513263	4934189	low temperature side vent of Azure Spring
Spray Geyser	7/31/10	12:45	510050	4930938	Multiple vents in pile of rocks and debris, discharges water constantly, height of eruption increases and decreases every few minutes
Steep Cone	8/5/10	12:30	510857	4934825	Clear, very hot, lots of bubbles, sits atop steep sided prominent cone (~8 m high)
Steep Cone	9/17/10	15:30	510857	4934825	"
Twin Butte Vista Spring	7/28/10	11:00	516089	4931392	Clear, very hot, splashes constantly at variable intensity.
Mammoth Hot Springs					
Boiling River	6/30/10	12:00	524502	4981344	River of hot water issues from cavern and flows ~50 m into the Gardner River.
Narrow Gauge Terrace	9/24/10	11:00	522904	4979625	Elaborate terrace of travertine formations. Sampled ponding pool about 2 m from fissure where there are active vents.
Other Springs					
Beryl Spring	9/22/10	13:00	520088	4947279	Clear, very hot. Next to road.
Soda Butte	5/30/10	8:30	566963	4969736	Old travertine terrace, now minimally active, little water discharge

200

APPENDIX (CONTINUED)

Table 2. USGS Stream Gauges where measurements of radionuclide activity in rivers were made.

Site Name	USGS Steam Gauge No.	Easting	Northing
Gibbon River at Madison Junction	06037100	511059	4943031
Firehole River at Madison Junction	06036905	510930	4940779
Firehole River at Old Faithful	06036805	514187	4922951
Gardner River at Mammoth Hot Springs	06191000	524392	4982164
Yellowstone River at Corwin Springs	06191500	516235	4995407

Table 3. Sites where radon and CO_2 efflux were measured in gas emissions.

Fumarole #	Date	Time	Easting	Northing	Comment
Amphitheater Springs					
AMPH1	5/27/10	10:20	521610	4961055	Group of fumaroles upslope of Solfatara Trail about 1/2 mile from trailhead.
AMPH2	5/27/10	11:00	521615	4961049	“
AMPH3	5/27/10	12:00	521621	4961066	“
AMPH4	5/27/10	13:00	521631	4961044	small footprint shaped vent uphill from AMPH3.
AMPH5	5/27/10	15:20	521520	4961070	Rain interrupted sampling. Had difficulty with water in RAD7 intake.
AMPH6	5/27/10	16:36	521513	4960688	AMPH6, AMPH7, and AMPH8 are in low valley southwest of the Solfatara Trail, along Lemonade Creek.
AMPH7	5/27/10	16:38	521477	4960685	“
AMPH8	5/27/10	16:41	521455	4960665	“
Mud Volcano					Fumaroles above Dragon's Mouth Spring, accessed by parking at Sulphur Cauldron and hiking uphill
MV1	5/28/10	9:20	544705	4951543	Powerful steam vent in large depression
MV2	5/28/10	9:25	544709	4941527	Hissing ground near MV1
MV3	5/28/10	10:15	544664	4941846	Small fumarole near MV4
MV4	5/28/10	10:20	544653	4941843	At bottom of hill, near road. Very active mudpot. Loud noises shake ground. Shoots mud 50 ft out of crater.
MV5	5/28/10	11:30	544737	4941703	On top of hill, near vigorously bubbling spring. Sampled two tiny fumaroles on either side.
MV6	5/28/10	11:45	544732	4941715	“
Norris Geyser Basin					
NOR1	6/1/10	13:45	522757	4952846	Small bubbling spring with no discharge. Located in sunken hole about 2 inches down.
NOR2	6/1/10	14:00	522765	4952829	Tiny hole in sinter platform. Uphill from NOR1, less water than NOR1. Hillside hisses with escaping gas.
Lower Geyser Basin					
LGB1	7/28/10	11:50	516112	4931377	Fumarole near Twin Butte Vista Spring
Lone Star Geyser Basin					
LST1	8/1/10	11:50	515011	4918060	Bubbling spring with raised sinter cone. Spring is 1-2 ft below the top of the cone.
LST2	8/1/10	13:55	515056	4918220	Sunken spring 8-10 inches below ground level.
LST3	8/1/10	14:25	515043	4918139	Small hole next to active splashing cone. About 6 inches down to water.
LST4	8/1/10	14:55	515044	4918134	Sunken spring about 6 inches down.
LST5	8/1/10	15:20	515038	4918130	Sunken spring about 5 inches down. Less active than LST3 and LST4
Rabbit Creek Hot Springs					
RCHS1	8/4/10	13:00	515003	4929811	Sunken hole in red dirt with steam rising.
RCHS2	8/4/10	13:25	515003	4929811	Close to, and similar to, RCHS1
RCHS3	8/4/10	14:00	515038	4929804	

201

APPENDIX (CONTINUED)

Table 4. Sites of rock sample collections.

ID	Location	Lithology	Date/Time	Easting	Northing
R1	Fawn Pass Trailhead	Madison Limestone	6/6/10 9:30	495360	4978090
R2	near Chocolate Pots	Lava Creek Tuff (A)	6/6/10 8:00	520752	4950991
R3	Lake Butte	Rhyodacite Porphyry	5/28/10 14:15	557491	4928718
R4	East of Lake Butte	Langford Formation (Alluvial Facies)	5/28/10 14:20	559333	4928902
R5	South of Lewis Falls	Plateau Rhyolite (Pitchstone Plateau Flow)	7/30/10 10:00	528354	4900102
R6	confluence of Spring Cr & FHR	Plateau Rhyolite (Scaup Lake Flow)	8/1/10 17:00	516215	4919188
R7	White Creek	Sinter	7/28/10 16:00	516059	4931221
R8	Gardner River Bridge	Mowry, Thermopolis, Kootenai, Fms	6/5/10 10:30	525330	4978509
R9	near Golden Gate	Huckleberry Ridge Tuff (A)	5/28/10 16:00	521873	4976009
R10	45th Parallel Bridge	P€ Schist & Hornfels	6/5/10 9:50	524159	4983901
R11	Campground Area	Older Travertine	6/5/10 10:00	524118	4980646
R12	Upper Terraces	Younger Travertine	6/5/10 11:00	522707	4978828
R13	Norris	Lava Creek Tuff (B)	6/1/10 9:15	523742	4952747
R14	West of Hydrophane Springs	Sinter	9/21/10 15:15	523047	4951893
R16	Thunderer Trailhead	Madison Limestone	5/30/10 11:35	571239	4974330
R17	Geode Creek	Geode Creek Basalt	5/30/10 12:50	540301	4973762
R18	Junction Butte	Jct. Butte Basalt	5/30/10 13:26	540073	4978570
R19	Mystic Falls	Plateau Rhyolite (Biscuit Basin Flow)	7/30/10 16:00	516099	4925680
R20	Duck Lake Overlook	Plateau Rhyolite (Elephant Back Flow)	7/30/10 12:20	532904	4918868

202

APPENDIX (CONTINUED)

Table 5. Geochemical and environmental parameters measured on-site at thermal springs.

Sample ID	Collection Date	pH	SC(µS/cm)	Temp(°C)	DO(mg/L)	Eh(volts)
Soda Butte	5/30/10	6.41	2611	23.0	1.3	-0.28
Cinder Pool	5/31/10	4.05	2100	85.5	---	0.35
“Cojones” West	5/31/10	2.41	2990	78.4	---	0.42
Perpetual Spouter	6/1/10	7.35	2520	91.5	---	0.02
"Acid Spring"	6/1/10	2.78	1465 +/- 5	89.0	---	0.43
Boiling River	6/30/10	6.33	1661	44.5	2.9	0.09
Ojo Caliente	7/27/10	7.72	1810	90.4	0.1	-0.27
Azure Spring	7/27/10	8.76	1749	77.3	0.4	-0.21
Bathtub Spring	7/27/10	8.97	1812	82.2	0.5	-0.28
Twin Butte Vista Spring	7/28/10	8.83	1623	91.0	0.1	-0.24
Mushroom Spring	7/28/10	7.98	1532	69.1	0.7	-0.02
Octopus Spring	7/28/10	8.05	1650	91.8	0.1	-0.19
Spray Geyser	7/31/10	8.60	1515	80.9	0.5	-0.17
Imperial Geyser	7/31/10	8.67	1581	75.4	0.6	-0.13
Rabbit Creek Source Pool	8/4/10	9.22	1977	85.3	0.3	-0.15
Scaffolding Pool	8/4/10	9.28	2074	89.3	0.2	-0.26
Steep Cone	8/5/10	7.94	1649	93.7	0	-0.29
Mound Spring	8/5/10	8.74	1655	93.9	0	-0.33
Perpetual Spouter	9/16/10	7.29	2380	87.5	---	-0.12
"Acid Spring"	9/16/10	3.03	1420	88.2	---	0.03
“Cojones” West	9/16/10	2.36	2960	78.5	---	0.05
Ojo Caliente	9/17/10	7.68	1485	--	---	-0.21
Steep Cone	9/17/10	7.88	1641	91.9	0.2	-0.20
Cinder Pool	9/20/10	4.18	2210	89.1	---	0.14
“Twin Bubblers” West	9/21/10	3.91	2108	79.3	0.7	-0.01
Medusa Spring	9/21/10	5.61	1400	81.5	---	0.05
Recess Spring	9/21/10	3.83	2110	84.8	---	0.10
Green Dragon Spring	9/21/10	2.9	1390	90.6	---	0.196
Beryl Spring	9/22/10	6.88	2010	90.5	---	-0.073
Narrow Gauge Terrace	9/24/10	7.8	2488	49.5	2.8	-0.0237

203

APPENDIX (CONTINUED)

Table 6, part I. Geochemical analysis of thermal spring water.

Sample ID	Date	HCO3	F	Cl	Br	NO3	SO4	As	Al	B	Ba	Be	Ca
Cinder Pool	5/31/10	0	6.747	592.82	1.892	<0.1	80.937	2.544	1.13	9.2	0.018	<0.0005	4.855
“Cojones” West	5/31/10	0	5.677	568.935	1.8	<0.1	342.46	2.428	2.46	8.55	0.023	<0.0005	4.46
Perpetual Spouter	6/1/10	15.5	6.751	792.318	2.45	<0.1	37.141	3.188	<0.08	11.7	0.01	0.0009	8.905
"Acid Spring"	6/1/10	0	0.608	287.978	0.879	<0.1	226.655	1.063	0.55	4.08	0.119	0.005	3.745
Boiling River	6/30/10	406	2.01	110	0.39	0.39	406	0.377	0.09	2.47	0.044	0.0007	184
Ojo Caliente	7/27/10	240	30.59	336	1.08	0.09	22.4	1.49	0.29	4.27	0.002	0.0009	0.813
Azure Spring	7/27/10	205	29.40	325	1.14	0.09	42.1	1.53	0.18	4.2	0.001	0.001	1.07
Bathtub Spring	7/27/10	222	30.73	332	0.14	0.09	26.9	0.489	0.20	4.37	0.002	0.001	0.814
Twin Butte Vista Spring	7/28/10	352	21.50	291	0.91	0.09	17.3	2.44	0.38	3.1	0.001	0.002	0.202
Mushroom Spring	7/28/10	292	16.94	262	0.89	0.09	19.8	1.95	0.20	2.76	0.0008	0.001	0.073
Octopus Spring	7/28/10	334	21.70	283	0.85	0.09	18.7	1.47	0.30	2.64	0.002	0.002	0.348
Spray Geyser	7/31/10	382	22.79	199	0.68	0.09	19.1	0.812	0.22	2.59	0.001	0.002	1.20
Imperial Geyser	7/31/10	392	23.01	207	0.77	0.09	22.1	0.915	0.37	2.74	0.001	0.004	1.06
Rabbit Creek Source Pool	8/4/10	380	26.55	312	1.02	0.09	17.4	1.78	0.26	3.27	0.002	<0.0005	0.347
Scaffolding Pool	8/4/10	377	28.37	333	1.11	0.09	15.8	1.8	0.32	3.53	0.002	0.0006	0.438
Steep Cone	8/5/10	293	30.03	260	0.39	0.09	18.5	1.14	0.31	3.62	0.005	0.001	0.232
Mound Spring	8/5/10	292	27.55	255	0.84	0.09	15.1	0.963	0.37	3.51	0.002	0.001	0.339
Perpetual Spouter	9/16/10	0	7.05	771.64	2.544	0.082	46.875	2.917	0.13	11.4	0.014	0.001	9.24
"Acid Spring"	9/16/10	0	0.54	284.47	0.924	0.427	212.298	1.088	0.61	4.34	0.115	0.005	4.035
“Cojones” West	9/16/10	0	1.892	538.32	1.701	<0.1	434.21	2.142	4.75	8.54	0.03	<0.0005	5.13
Ojo Caliente	9/17/10	227	30.079	327.015	1.033	0.104	23.704	1.434	0.23	4.38	<0.0008	0.0008	0.8765
Steep Cone	9/17/10	294	28.0	278	0.90	0.09	15.7	1.14	0.31	3.54	0.007	0.001	0.189
Cinder Pool	9/20/10	0	7.67	649.01	1.98	<0.1	80.89	1.364	0.93	9.5	0.02	<0.0005	5.455
“Twin Bubblers” West	9/21/10	0.00	4.87	542	1.83	0.09	94.6	1.74	2.06	8.05	0.166	0.002	3.30
Medusa Spring	9/21/10	7.01	5.166	433.568	1.343	0.03	49.858	1.436	<0.08	7.42	0.032	0.001	2.44
Recess Spring	9/21/10	0	5.853	656.56	2.083	0.03	98.228	2.245	1.12	10.4	0.023	<0.0005	6.54
Green Dragon Spring	9/21/10	0	4.315	273.1	0.838	0.03	256.213	1.077	3.58	4.81	0.044	0.003	3.565
Beryl Spring	9/22/10	107	18.804	572.125	1.781	0.03	71.969	2.924	0.19	7.56	0.001	0.0009	3.845
Narrow Gauge Terrace	9/24/10	400	2.37	174	0.55	0.09	607	0.631	<0.08	4.01	0.051	0.001	313

204

APPENDIX (CONTINUED)

Table 6, part II. Geochemical analysis of thermal spring water (continued).

Sample ID	Date	Fe	K	Li	Mg	Mn	Mo	Na	Sb	Si as SiO2	Sr	Zn
Cinder Pool	5/31/10	0.019	43	3.51	0.021	0.004	0.086	357	0.03	392	0.016	0.008
Crystal Spring west	5/31/10	0.181	22.5	3.54	0.0295	0.011	0.135	346	0.097	325	0.012	<0.002
Perpetual Spouter	6/1/10	0.028	41.8	5.02	0.0605	0.033	0.065	449	0.114	290	0.032	<0.002
"Acid Spring"	6/1/10	6.77	52.1	1.09	0.479	0.139	<0.005	181	0.026	454	0.02	0.068
Boiling River	6/30/10	<0.003	27.8	0.778	52.7	0.008	0.026	83.7	<0.02	38.7	1.3	0.005
Ojo Caliente	7/27/10	<0.003	9.2	3.02	<0.002	<0.001	0.035	312	<0.02	207	0.006	<0.002
Azure Spring	7/27/10	<0.003	10.6	2.21	<0.002	<0.001	0.06	297	0.037	223	0.008	<0.002
Bathtub Spring	7/27/10	<0.003	10.8	2.51	<0.002	<0.001	<0.005	320	<0.02	221	0.007	<0.002
Twin Butte Vista Spring	7/28/10	<0.003	10.4	2.78	<0.002	<0.001	0.021	320	0.057	260	<0.0007	<0.002
Mushroom Spring	7/28/10	<0.003	16.9	1.51	<0.002	<0.001	0.021	279	0.042	263	<0.0007	<0.002
Octopus Spring	7/28/10	<0.003	13.3	2.51	<0.002	<0.001	0.02	294	0.034	243	<0.0007	<0.002
Spray Geyser	7/31/10	0.008	9.77	1.74	0.020	<0.001	0.019	286	<0.02	215	0.001	<0.002
Imperial Geyser	7/31/10	<0.003	12	1.87	0.011	<0.001	0.017	295	<0.02	211	0.003	<0.002
Rabbit Creek Source Pool	8/4/10	<0.003	12	3.99	0.013	<0.001	0.022	362	0.051	223	0.002	<0.002
Scaffolding Pool	8/4/10	<0.003	13.4	4.2	0.086	<0.001	0.023	367	0.055	241	0.002	<0.002
Steep Cone	8/5/10	<0.003	10.6	1.3	0.011	<0.001	0.022	306	<0.02	318	<0.0007	<0.002
Mound Spring	8/5/10	<0.003	9.72	1.18	0.010	<0.001	0.015	307	<0.02	323	<0.0007	<0.002
Perpetual Spouter	9/16/10	0.188	41.4	5.01	0.0625	0.037	0.084	466	0.108	286	0.033	<0.002
"Acid Spring"	9/16/10	7.2431	50.7	0.952	0.5165	0.152	<0.005	191	0.022	395	0.022	0.074
Cojones West	9/16/10	0.274	21.9	3.52	0.0575	0.014	0.09	345	0.084	275	0.013	<0.002
Ojo Caliente	9/17/10	<0.002	7.7	3.18	<0.002	<0.001	0.039	342	<0.02	238	0.006	<0.002
Steep Cone	9/17/10	0.004	10.3	1.33	<0.002	0.001	0.025	298	<0.02	341	<0.0007	<0.002
Cinder Pool	9/20/10	0.023	44.3	3.39	0.027	0.005	0.062	362	<0.02	352	0.018	<0.002
Twin Bubblers West	9/21/10	1.01	47.2	3.44	0.148	0.043	0.027	301	0.028	344	0.02	0.077
Medusa Spring	9/21/10	0.01	26.5	2.62	0.0895	0.314	0.033	272	0.103	318	0.005	<0.002
Recess Spring	9/21/10	0.041	34.4	4.02	0.0725	0.025	0.103	389	0.057	404	0.016	<0.002
Green Dragon Spring	9/21/10	1.228	39.5	1.63	0.3815	0.187	0.027	191	0.061	379	0.012	0.018
Beryl Spring	9/22/10	0.006	17.8	4.55	0.0115	0.016	0.127	417	0.047	269	0.007	<0.002
Narrow Gauge Terrace	9/24/10	0.016	42.2	1.24	76.2	0.018	0.035	134	<0.02	53.1	1.66	<0.0

205

APPENDIX (CONTINUED)

Table 7. Radon activities, activity ratios, and CO_2 fluxes measured in fumarolic gas.

Fumarole #	(^{220}Rn) dpm/L	(^{220}Rn) +/-	(^{222}Rn) dpm/L	(^{222}Rn) +/-	(^{220}Rn/^{222}Rn)	ratio +/-	CO_2 flux (g m^{-2} d^{-1})
AMPH1	17	27	36	6	0.46	0.46	461
AMPH2	28	31	15	2	1.83	1.83	1642
AMPH3	5	2	36	6	0.14	0.07	329
AMPH4	81	46	81	21	1.01	0.62	1641
AMPH5	48	37	23	9	2.06	1.77	240
AMPH6	20	27	78	18	0.25	0.25	490
AMPH7	79	46	80	19	0.98	0.61	2398
AMPH8	64	45	22	4	2.91	2.10	2398
MV1	63	42	92	24	0.68	0.49	839
MV2	160	60	213	33	0.75	0.31	1869
MV3	25	30	317	13	0.08	0.08	21
MV4	317	84	109	49	2.92	1.53	31
MV5	96	49	73	21	1.31	0.77	74
MV6	160	59	359	42	0.45	0.17	902
NOR1	161	59	65	19	2.47	1.17	51
NOR2	353	84	52	15	6.74	2.54	136
LGB1	160	34	18	12	8.94	6.14	225
LST1	667	71	2201	106	0.30	0.04	678
LST2	15	17	267	30	0.06	0.06	994
LST3	272	54	315	40	0.86	0.20	3601
LST4	315	48	482	49	0.65	0.12	1247
LST5	2	12	474	48	0.00	0.00	3831
RCHS1	81	31	10	7	8.20	6.41	718
RCHS2	24	20	2	5	9.65	9.25	54
RCHS3	71	21	11	8	6.33	4.95	26

APPENDIX (CONTINUED)

Table 8. Radionuclide activities measured in thermal spring water.

Sample ID	Date	(^{220}Rn) dpm/L	(^{222}Rn) dpm/L	(^{224}Ra) dpm/L	(^{223}Ra) dpm/L	(^{228}Ra) dpm/L	(^{226}Ra) dpm/L
Cinder Pool	5/31/10	--	796.24	--	--	2.51	0.11
"Cojones" West	5/31/10	--	158.40	--	--	2.81	0.10
Perpetual Spouter	6/1/10	--	--	--	--	2.68	0.68
"Acid Spring"	6/1/10	--	--	--	--	16.92	0.21
Boiling River	6/30/10	88.75	2606.14	--	--	5.87	1.39
Ojo Caliente	7/27/10	5.55	151.30	0.1557	0.0021	0.23	0.06
Azure Spring	7/27/10	14.11	144.70	0.4269	0.0014	3.86	0.09
Bathtub Spring	7/27/10	9.95	36.63	0.4027	0.0017	0.76	0.09
Twin Butte Vista Spring	7/28/10	0.46	2.12	0.0221	0.0003	0.27	0.05
Mushroom Spring	7/28/10	3.04	134.42	0.0404	0.0005	0.20	0.11
Octopus Spring	7/28/10	2.57	140.76	0.0508	0.0004	0.18	0.10
Spray Geyser	7/31/10	4.45	7.07	0.0732	0.0027	0.22	0.06
Imperial Geyser	7/31/10	1.49	0.95	0.1300	0.0012	0.20	0.10
Rabbit Creek Source Pool	8/4/10	1.01	0.22	0.1106	0.0004	0.19	0.13
Scaffolding Pool	8/4/10	--	--	0.0868	0.0006	0.23	0.11
Steep Cone	8/5/10	--	--	0.0111	0.0002	0.05	0.11
Mound Spring	8/5/10	--	--	0.0053	0.0001	0.07	0.04
Perpetual Spouter	9/16/10	222.55	108.23	0.4726	0.0351	3.01	0.11
"Acid Spring"	9/16/10	35.41	18.60	14.5878	0.6208	20.90	0.17
"Cojones" West	9/16/10	182.95	109.29	5.5730	0.4599	1.74	--
Ojo Caliente	9/17/10	2.11	200.08	0.1325	0.0020	0.17	0.09
Steep Cone	9/17/10	35.42	729.64	0.0239	0.0006	0.08	0.10
Cinder Pool	9/20/10	3.19	106.08	10.6925	0.1475	2.51	0.09
"Twin Bubblers" West	9/21/10	6.22	97.81	10.6601	0.1599	15.98	0.24
Medusa Spring	9/21/10	2.27	23.41	3.1927	0.0327	4.06	0.05
Recess Spring	9/21/10	5.98	69.94	10.5007	0.1029	5.08	0.12
Green Dragon Spring	9/21/10	12.52	--	6.2270	0.1409	5.14	0.14
Beryl Spring	9/22/10	1.73	12.62	0.9194	0.0060	0.71	0.07
Narrow Gauge Terrace	9/24/10	4.62	4.59	21.4745	3.1320	13.15	1.39

207

APPENDIX (CONTINUED)

Table 9. Relevant activity ratios in thermal spring water and CO_2 fluxes measured with the modified accumulation chamber.

Sample ID	Date	($^{220}Rn/^{222}Rn$)	($^{220}Rn/^{224}Ra$)	($^{224}Ra/^{222}Rn$)	($^{224}Ra/^{223}Ra$)	($^{224}Ra/^{228}Ra$)	($^{228}Ra/^{226}Ra$)	CO_2 flux (g m^{-2} d^{-1})
Soda Butte	5/30/10	--	--	--	--	--	--	60*
Cinder Pool	5/31/10	--	--	--	--	--	21.91	--
“Cojones” West	5/31/10	--	--	--	--	--	27.46	82*
Perpetual Spouter	6/1/10	--	--	--	--	--	3.92	2*
"Acid Spring"	6/1/10	1.58	--	--	--	--	79.08	80*
Boiling River	6/30/10	0.03	--	--	--	--	4.22	1802
Ojo Caliente	7/27/10	0.04	35.64	0.0010	73.52	0.68	3.54	398**
Azure Spring	7/27/10	0.10	33.04	0.0030	298.47	0.11	42.91	13**
Bathtub Spring	7/27/10	0.27	24.70	0.0110	237.83	0.53	8.66	--
Twin Butte Vista Spring	7/28/10	0.22	20.93	0.0104	76.55	0.08	4.91	--
Mushroom Spring	7/28/10	0.02	75.32	0.0003	74.18	0.20	1.76	45**
Octopus Spring	7/28/10	0.02	50.66	0.0004	128.39	0.28	1.85	--
Spray Geyser	7/31/10	0.63	60.78	0.0103	27.26	0.33	3.79	39**
Imperial Geyser	7/31/10	1.57	11.43	0.1371	109.10	0.65	2.10	16**
Rabbit Creek Source Pool	8/4/10	4.57	9.16	0.4984	277.35	0.58	1.41	4
Scaffolding Pool	8/4/10	--	--	--	144.81	0.38	2.14	9
Steep Cone	8/5/10	--	--	--	59.36	0.22	0.46	1953
Mound Spring	8/5/10	--	--	--	63.03	0.08	1.87	138
Perpetual Spouter	9/16/10	2.06	470.90	0.0044	13.45	0.16	28.58	731
"Acid Spring"	9/16/10	1.90	2.43	0.7843	23.50	0.70	122.82	312
Cojones West	9/16/10	1.67	32.83	0.0510	12.12	3.20	--	45
Ojo Caliente	9/17/10	0.01	15.94	0.0007	65.49	0.78	1.96	3811
Steep Cone	9/17/10	0.05	1483.42	0.0000	36.97	0.30	0.80	1649
Cinder Pool	9/20/10	0.03	0.30	0.1008	72.51	4.26	28.88	3909
“Twin Bubblers” West	9/21/10	0.06	0.58	0.1090	66.65	0.67	66.00	15
Medusa Spring	9/21/10	0.10	0.71	0.1364	97.69	0.79	76.67	464
Recess Spring	9/21/10	0.09	0.57	0.1501	102.02	2.07	42.00	934
Green Dragon Spring	9/21/10	--	2.01	--	44.19	1.21	37.91	212
Beryl Spring	9/22/10	0.14	1.89	0.0728	151.98	1.29	10.03	2832
Narrow Gauge Terrace	9/24/10	1.01	0.22	4.6784	6.86	1.63	9.47	--

* - From nearby soil with accumulation chamber
** - Used modified accumulation chamber without return tube from detector to bottle